Published in final edited form as:

Nature. 2010 July 8; 466(7303): 248–252. doi:10.1038/nature09151.

A random cell motility gradient downstream of FGF controls elongation of an amniote embryo

Bertrand Bénazéraf[1,2,6], **Paul Francois**[3], **Ruth E. Baker**[4], **Nicolas Denans**[2,6], **Charles D. Little**[5], and **Olivier Pourquie**[1,2,5,6]

[1] Howard Hughes Medical Institute, Kansas City, Missouri 64110, USA

[2] Stowers Institute for Medical Research, Kansas City, Missouri 64110, USA

[3] Center for Studies in Physics and Biology, The Rockefeller University, New York New York 10065, USA

[4] Centre for Mathematical Biology, Mathematical Institute, University of Oxford, 24-29 St Giles', Oxford OX1 3LB, UK

[5] Department of Anatomy and Cell Biology, University of Kansas Medical Center, Kansas City, Kansas 66160, USA

[6] Institut de Génétique et de Biologie Moléculaire et Cellulaire (IGBMC), CNRS (UMR 7104), Inserm U964, Université de Strasbourg, Illkirch. F-67400, France

Abstract

Vertebrate embryos are characterized by an elongated antero-posterior (AP) body axis, which forms by progressive cell deposition from a posterior growth zone in the embryo. Here, we used tissue ablation in the chicken embryo to demonstrate that the caudal presomitic mesoderm (PSM) plays a key role in axis elongation. Using time-lapse microscopy, we analysed the movements of fluorescently labelled cells in the PSM during embryo elongation which revealed a clear posterior-to-anterior gradient of cell motility and directionality in the PSM. We tracked the movement of the PSM extracellular matrix in parallel with the labelled cells and subtracted the extracellular matrix movement from the global motion of cells. After subtraction, cell motility remained graded but lacked directionality, indicating that the posterior cell movements associated with axis elongation in the PSM are not intrinsic but reflect tissue deformation. The gradient of cell motion along the PSM parallels the fibroblast growth factor (FGF)/mitogen-activated protein kinase (MAPK)

Corresponding Author: Olivier Pourquié, Ph.D. Institut de Génétique et de Biologie Moléculaire et Cellulaire (IGBMC), CNRS (UMR 7104), Inserm U964, Université de Strasbourg, Illkirch. F-67400, France. Phone: 33 3 88 65 32 16, pourquie@igbmc.fr.

Supplementary Information is linked to the online version of the paper at www.nature.com/nature.

Author Information

Reprints and permission information are available at www.nature.com/reprints.

Author Contributions

BB and OP designed the biological experiments. BB and ND performed the biological experiments. CDL gave technical and theoretical support for the time-lapse experiments. PF, ND, BB and OP analysed the biological experiments; in particular, PF designed the tracking programs, tracked cells and ECM motions, and performed the random walk analysis. REB designed, analysed and simulated the mathematical models in collaboration with BB, PF and OP. BB, OP, REB and PF wrote the manuscript. All authors discussed the results and commented on the manuscript. OP supervised the project.

gradient [1], which has been implicated in the control of cell motility in this tissue[2]. Both FGF signalling gain- and loss-of-function experiments lead to disruption of the motility gradient and a slowing down of axis elongation. Furthermore, embryos treated with cell movement inhibitors (Blebbistatin or RhoK inhibitor), but not cell cycle inhibitors, show a slower axis elongation rate. We propose that the gradient of random cell motility downstream of FGF signalling in the PSM controls posterior elongation in the amniote embryo. Our data suggest that tissue elongation is an emergent property that arises from the collective regulation of graded, random cell motion rather than by the regulation of directionality of individual cellular movements.

During the formation of the anterior-most tissues in amphibians, the embryonic tissue narrows and elongates posteriorly through a process called convergence/extension. This process, involves cellular intercalation and is often considered to be the mechanism driving vertebrate axis elongation[3]. In amniotes, convergence/extension movements are associated with early stages of primitive streak and axis formation[4–6]. Large-scale convergence movements become progressively less important during trunk and tail formation, which derive from the regressing tail bud, the width of which changes little during development. Therefore, the nature of the mechanism underlying posterior elongation of the embryonic axis remains unknown.

Although the ectopic graft of a node (the amniote equivalent of the Spemann organizer) can lead to the formation of an elongated, ectopic embryonic axis[7, 8], the node itself is unnecessary for body elongation[9–11]. To identify the structure(s) controlling the axis elongation process, we performed laser ablations of various caudal regions in cultured Hamburger and Hamilton (HH) stage 10–11 chicken embryos[12]. We then replaced the deleted tissue with a piece of agarose gel to avoid any interference from the contractile ring generated by the wound healing response[13] and measured the axis elongation rate using time-lapse microscopy (Fig. 1). Strikingly, bilateral deletion of the posterior presomitic mesoderm (PSM), which lies on both sides of the anterior primitive streak and Hensen's node has a stronger effect on axis elongation than deletion of the axial structures, of anterior parts of the PSM or of the lateral plate compared to non-operated embryos ($P < 0.01$, $n = 3$ to 5 for each condition) (Fig. 1a–c and Supplementary Movies 1–4). To analyse cellular movements in the posterior PSM, the anterior primitive streak and epiblast of stage 4–5 HH chicken embryos were electroporated with a plasmid coding for the nuclear marker H2B GFP and the fluorescently labeled descendants were tracked over time [14]. Cells in the caudal PSM exhibited high motility and important cell mixing[2, 15]($n = 4$; Fig. 2a and Supplementary Movie 5). The directionality of cells within the PSM was quantified using a formed somite as a fixed reference point. Cell movements exhibited a posterior directional bias in the whole tissue and convergence toward the axis in the anterior part of each PSM (Fig. 2a). We observed a clear motility gradient decreasing in a posterior-to-anterior direction along the PSM (n =4/4 embryos; Fig. 2d). Analysis of cell counts on sagital sections (data not shown) of the PSM or fluorescence intensity in Hoechst-labeled embryos reveals a cell density gradient, opposite to the cellular motility gradient (Supplementary Fig. 1a,b).

To quantify the apparent movement of PSM cells resulting from the tissue deformation (i.e., elongation) versus their local movement within the tissue, we measured cell movement relative to the local extracellular matrix (ECM). As a marker for ECM, we used Fibronectin, which is produced by ectoderm cells and forms a network of fibrils surrounding the PSM cells[16]. Embryos electroporated with H2B-GFP were co-labelled with an anti-Fibronectin antibody coupled to an Alexa-555 fluorochrome. Using time-lapse microscopy, ECM tissue movement and the cellular movements in the PSM during axis extension were recorded in double-labelled embryos (n = 4; Fig. 2a, b and Supplementary Movie 6)[17, 18]. The tracked Fibronectin fibers show almost the same pattern of directional displacement (extension and anterior convergence) as the cells (Fig. 2b). To examine cellular movements relative to the ECM, we subtracted Fibronectin movements from the observed cellular movements. We consistently observed a decreasing posterior-to-anterior gradient of local cell motility within the PSM (n = 4/4 embryos; Fig. 2c, e). Surprisingly, the movements of cells relative to the ECM did not show any local directional bias (Fig. 2c). The mean square displacement of these cells compared to the Fibronectin movement scales with time (Fig. 2f, g), suggesting that cells exhibit a "random walk"-like diffusive behaviour[19], with the diffusion of cells relative to the Fibronectin following a posterior-to-anterior gradient (Fig. 2g). A physical analogy can be made by comparing cells with fluid molecules (diffusion would then be a measure of thermal agitation), indicating a posterior-to-anterior effective temperature gradient in the PSM. We tracked the movement of a second ECM protein, Fibrillin2, using the same strategy[20]. Subtracting the movement of the two ECM components or subtracting the mean movement of cells (see Supplementary Methods) from the Fibronectin movement gave a net movement that is virtually null (Supplementary Fig. 2, Supplementary Movie 7). Thus, both Fibronectin and Fibrillin2 motion accurately reflect ECM motion and tissue deformation.

We then investigated the orientation of cell protrusions relative to the AP axis following electroporation of a membrane-tethered GFP in the PSM. Statistical analyses demonstrated that the distribution of angles between the major lamelliform protrusion of cells and the AP body axis does not differ from a random distribution (Chi-squared test [$P>0.05$] and Kuiper's test $1.7229<1.747$ [critical value]), consistent with the lack of directionality of local cellular movements (Fig. 2h–j and Supplemental Methods). These observations rule out chemotactic or convergence/extension cellular behaviours, which are associated with directed cellular movements and protrusion orientation relative to the body axis. We conclude that PSM cells exhibit a gradient of random motility relative to the ECM.

Cellular motility in the PSM is controlled by a posterior-to-anterior gradient of FGF/MAPK signalling[2]. Progenitors entering the posterior PSM express FGF8, thus potentially triggering the active, random movements observed[1, 2]. We blocked FGF signalling by electroporating a dominant-negative version of the FGF receptor (FGFR1dn) in PSM cells[21]. Because FGF signalling is required for mesoderm ingression from the epiblast[22, 23], we used an inducible promoter that allowed expression of the transgene to occur after the electroporated cells had entered the PSM[24]. In cells overexpressing FGFR1dn, the motility of cells before and after tissue movement subtraction was diminished compared to controls (n = 3/3 embryos; Supplementary Fig. 3a–c and Supplementary Movie 8). A shallower

motility gradient and a decrease in the elongation rate compared to controls were observed in the FGFR1dn-expressing embryos ($P < 0.001$, $n = 10$; Fig. 3a–b and Supplementary Movie 8). A severe reduction of tissue convergence movements ($P < 0.05$, $n = 10$, Fig. 3c and Supplementary Movie 8) but no effect on the density gradient (Fig. 3d) were observed in these embryos. We repeated this experiment along with a deletion of the primitive streak region and observed a diminution of the elongation rate in these embryos compared to controls, thus ruling out the role of gastrulation defects (Supplementary Fig. 4a). Additionally, we chemically inhibited the FGF pathway using the FGFR1 inhibitor SU5402 and observed a significant slowing down of axis elongation in the treated embryos (Supplementary Fig. 4b). These data suggest that FGF-dependent cellular movements are necessary for tissue elongation.

We then examined the effect of overactivating the FGF pathway on posterior axis elongation following electroporation of an FGF8-expressing construct in PSM precursors. Tracking the PSM cells demonstrated that the motility gradient is disrupted due to a high level of random cell motility maintained in the anterior PSM ($n = 3/3$ embryos; Supplementary Fig. 3d–f, Fig 3f and Supplementary Movie 9). Surprisingly, the elongation rate was significantly reduced compared to control embryos ($P < 0.01$, $n = 5$; Fig. 3e and Supplementary Movie 9). Further, the tissue undergoes less convergence and expands laterally compared to control embryos ($P < 0.05$, $n = 5$; Fig. 3g, Supplementary Fig. 5 and Supplementary Movie 9). Therefore, FGF signalling is necessary and sufficient for the graded, random movements of cells observed along the PSM. Although FGF signalling gain- and loss-of-function elicit opposite effects on cellular motility in the PSM, both experimental procedures decrease the rate of embryo elongation.

To ascertain whether the effects on axis elongation resulted from the alteration of cell motility downstream of FGF signalling and not from other properties of the FGF gradient, we treated embryos with the Rho-Kinase inhibitor Y27632 or with Blebbistatin (an inhibitor of Myosin II phosphorylation), both of which inhibit cell motility. As observed in the FGF gain- and loss-of-function experiments, expression of the posterior PSM marker *Mesogenin 1* (*Msgn1*) and of the cyclic gene *Lunatic fringe* (*Lnfg*) were unaffected (Supplementary Fig. 6), and somites continued to form in treated embryos. However, the cell motility gradient was disrupted, and axis elongation and convergence were diminished (n=3 embryos for both conditions; Fig. 3i–l, Supplementary Fig. 7a–d, i–j Supplementary Movie 10, 11). The cell motility inhibition phenocopies the FGF loss-of-function experiments, suggesting that the effect of FGF on elongation is mainly due to its action on cell movements. Therefore, the FGF-dependent gradient of cellular motility in the PSM plays a key role in elongation of the embryo.

FGF signalling is known to control proliferation, raising the possibility that proliferation in the posterior PSM might play a role in the control of axis elongation. We examined the cell-cycle status in propidium iodide-labelled dissociated cells of the different caudal regions in chicken embryo (Supplementary Fig. 8a–c). This analysis did not identify a major posterior proliferation center that could drive axis elongation. Furthermore, FGF gain- and loss-of-function experiments did not show major differences in cell cycle phase distribution compared to wild type conditions. (Supplementary Fig. 8d–h). To test directly the role of

cell proliferation on the control of axis elongation, we treated embryos with Mitomycin C (which blocks cells in the G1 phase) or Aphidicolin (an S-phase inhibitor) and measured the elongation rate in treated embryos. In both cases, although cell proliferation was strongly reduced, no effect on axis elongation was observed (n=3 for each condition; Fig. 3m–p, Supplementary Fig. 7e–h and Supplementary Movies 12–13). Modelling migratory cell behaviour in neural cells demonstrates that directional movements of cells similar to those resulting from chemotaxis can be elicited by gradients of motogenic substances[25]. The directional movements of posterior PSM cells can be explained using models in which cellular motility in the PSM is equated to diffusion (Box 1). Exposing cells to a gradient of a motility-promoting substance (e.g., FGF) results in an initial global asymmetric displacement of the cells toward the source of the gradient and establishes a cellular density gradient opposed to the gradient of motility (Box 1 and Supplementary Movie 15). Overexpressing FGF8 *in vivo* not only abolishes the gradient of cell motility and the biased directional movements but also flattens and lowers the cell density gradient as predicted by the simulations based on diffusion models (n = 4; Fig. 3h; Box 1 and Supplementary Movie 16). It is tempting, therefore, to speculate that in the PSM, as cellular density increases anteriorly, the resistance to expansion also increases, thus synergizing with the cellular movements to bias tissue expansion toward the posterior end of the embryo (Fig. 3q). This hypothesis implies the existence of boundaries that prevent the lateral expansion of the PSM tissue. Increased cell density on both sides of the PSM is consistent with the existence of such boundaries (Supplementary Fig. 1a,c). In embryos overexpressing FGF8, these boundaries are displaced laterally, leading to increased width, consistent with a dilatation of the tissue (Supplementary Fig. 5). In contrast to the convergent mechanism proposed to cause elongation of the anterior-most structures in vertebrates, here, the convergence of cells in the PSM is mostly passive. Just as a rubber band narrows when it is stretched, the anterior PSM exhibits convergent motion due to forces generated by posterior expansion of the tissue. Our simulations illustrate that imposing a gradient of random motility on a cell population can lead to unexpected behaviours such as a directional movement of the population of cells along the gradient and the establishment of a gradient of cell density opposite to the resulting movement. This strikingly mirrors the situation in the posterior PSM, which led us to propose that such a directional cell migration along the FGF/MAPK gradient provides the basis for axis extension. A biologically accurate model for this process will need to take into account the generation of forces responsible for elongation.

Box 1

Modelling of cell motility

To test hypotheses arising from the *in vivo* experiments we constructed a mathematical model of cell movements in the PSM. We investigated, using a stochastic, individual-based model, whether the hypothesized effect of FGF signalling on cell motility can lead to the directed movement of cells in the PSM and to the gradient of cell density observed *in vivo* (for more details of the model see the Supplementary Methods). On an individual level, we assume that each cell acts as a random walker, moving according to a space-jump process on a two-dimensional lattice imposed on the PSM. We consider the PSM as a stationary window and explore the relationship between cell density and the transition

probabilities of the space-jump process. We supposed first that the transition rates (per unit time) of moving left, right, up or down depend only on the cell density in the box into which cells could move. Cell movements were simulated using the stochastic simulation algorithm (SSA)[26] and the results are shown in Box 1, Fig. 1(a). One side of the PSM is shown, with posterior on the left and anterior on the right of each plot. Random motility leads to a symmetric wave of cell movements.

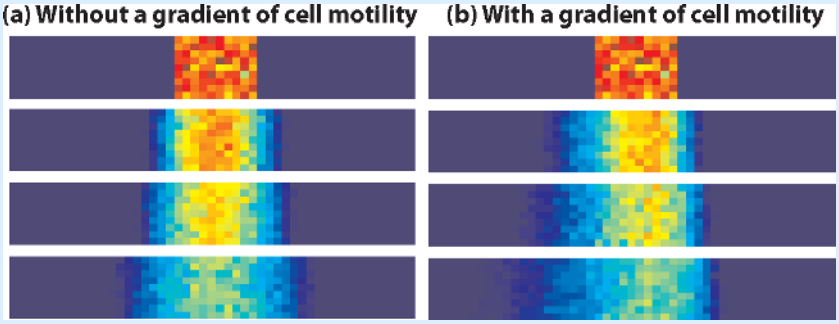

Box 1 Figure 1.
Simulation results at t=0,50,100,250

We then used the same model to test the hypothesized effects of Fgf8 on cell movements by imposing a gradient of cell motility across the domain with high motility posteriorly and lower motility anteriorly. The transition rates for each box were assumed to be dependent on the level of FGF signalling in that box (as well as dependent on cell density in the neighbouring boxes) and we used the SSA to simulate cell movement with the modified transition rates. In contrast to the control case, the gradient of FGF signalling leads to a gradient of cell motility along the PSM: cells are more likely to move in regions where levels of FGF signalling are higher. The outcome is the cell density profile shown in Box 1, Fig. 1(b). Greater displacements occur posteriorly and, as a result, we see higher cell density anteriorly. An illustration of the phenomenon of directional diffusion can be obtained by imposing a gradient of temperature upon a drop of india ink/glycerol diffusing in water (Supplementary Movie 14).

Axis formation by outgrowth is a common morphogenetic strategy that is widely evident in animals and plants. Thus, the mechanism described here might apply to other well-characterized, polarized axes, such as the limb buds, in which a similar FGF/MAPK gradient is established along the proximo-distal axis.

Methods Summary

Chicken embryo preparation

Fertilized chicken eggs were obtained from commercial sources. Embryos were prepared for EC (Early Chick) cultures[27] and then electroporated and/or ablated followed by culture on the microscope stage for time-lapse recordings. Embryos were staged as described[12].

Embryo staining and time-lapse microscopy

In vitro electroporations were carried out as described in the Supplementary Methods. H2B-GFP plasmid is a gift from Dr. Rusty Landford (Caltech). A monoclonal antibody to avian Fibronectin, B3D6 (Developmental Studies Hybridoma Bank, University of Iowa, Iowa City, IA) was directly coupled to a fluorochrome Alexa-555 (Molecular Probes, Eugene, OR) and microinjected into the PSM and lateral mesoderm 1 h before the start of a time-lapse experiment. Time-lapse microscopy and image treatment were accomplished as described[28, 29] and in the Supplementary Methods.

Functional experiments

The pMIW cFGF8b expression vector[30] was co-electroporated with H2B-GFP plasmid. A fragment corresponding to the Xenopus FGFRdn (XFD) (gift from Dr Patrick Lemaire as described [21]) was cloned into pBI-EGFP (Clontech). For the inducible constructs, pBI-EGFP or pBI-FGFRdn was coelectroporated with pCIRX-rtTA-Advanced (gift from Dr Tadahiro Iimura). A version of the pBI vectors devoid of GFP and rtTA-Advanced without red fluorescent protein was also used in order to facilitate tracking of co-electroporated H2B-GFP or Fibronectin Antibody.

Full Methods and any associated references are available in the online version of this paper at www.nature.com/nature.

Supplementary Material

Refer to Web version on PubMed Central for supplementary material.

Acknowledgments

The authors thank R Li, D Roellig and members of the Pourquié laboratory for critical reading of the manuscript. The authors acknowledge E Siggia for support, B Rongish, M Filla, C Cui, A Peterson, K Perko, R Alexander, R Fender, JD Fauny, T Cheuvront, and members of the IGBMC imaging center for assistance with imaging-related techniques. We thank L Kennedy and T Iimura for help with the experiments, and the members of the Cytometry Facility at the Stowers Institute for Medical Research for assistance. We thank S Leblanc, H Li, N Wicker and P Moncuquet for help with statistical analysis. The authors thank S Esteban for artwork and J Chatfield for editorial assistance. This research was supported by the Howard Hughes Medical Institute, the Stowers Institute for Medical Research, NIH grant R02 HD043158 and a Chaire d'excellence to OP. PF is supported by NSF grant DMR-0129848 (attributed to E Siggia) and Lavoisier Fellowship. REB is supported by an RCUK Fellowship in Mathematical Biology and a Microsoft European Postdoctoral Research Fellowship.

References

1. Dubrulle J, Pourquie O. fgf8 mRNA decay establishes a gradient that couples axial elongation to patterning in the vertebrate embryo. Nature. 2004; 427:419–422. [PubMed: 14749824]
2. Delfini MC, Dubrulle J, Malapert P, Chal J, Pourquie O. Control of the segmentation process by graded MAPK/ERK activation in the chick embryo. Proc Natl Acad Sci USA. 2005; 102:11343–11348. [PubMed: 16055560]
3. Keller R, Shook D, Skoglund P. The forces that shape embryos: physical aspects of convergent extension by cell intercalation. Physical biology. 2008; 5:15007.
4. Lawson A, Schoenwolf GC. New insights into critical events of avian gastrulation. Anat Rec. 2001; 262:238–252. [PubMed: 11241193]

5. Voiculescu O, Bertocchini F, Wolpert L, Keller RE, Stern CD. The amniote primitive streak is defined by epithelial cell intercalation before gastrulation. Nature. 2007; 449:1049–1052. [PubMed: 17928866]
6. Yang X, Dormann D, Munsterberg AE, Weijer CJ. Cell movement patterns during gastrulation in the chick are controlled by positive and negative chemotaxis mediated by FGF4 and FGF8. Dev Cell. 2002; 3:425–437. [PubMed: 12361604]
7. Beddington RS. Induction of a second neural axis by the mouse node. Development. 1994; 120:613–620. [PubMed: 8162859]
8. Waddington CH. Experiments on the development of chick and duck embryos cultivated in vitro. Phil Trans R Soc Land. 1932; B221:179–230.
9. Charrier JB, Teillet MA, Lapointe F, Le Douarin NM. Defining subregions of Hensen's node essential for caudalward movement, midline development and cell survival. Development. 1999; 126:4771–4783. [PubMed: 10518494]
10. Bellairs R. The development of somites in the chick embryo. J Embryol Exp Morphol. 1963; 11:697–714. [PubMed: 14081990]
11. Spratt NT Jr. Analysis of the organizer center in the early chick embryo. I. Localisation of prospective notochord and somite cells. J Exp Zool. 1955; 128:121–162.
12. Hamburger V. The stage series of the chick embryo [comment]. Dev Dyn. 1992; 195:273–275. [PubMed: 1304822]
13. Martin P, Lewis J. Actin cables and epidermal movement in embryonic wound healing. Nature. 1992; 360:179–183. [PubMed: 1436096]
14. Sbalzarini IF, Koumoutsakos P. Feature point tracking and trajectory analysis for video imaging in cell biology. Journal of structural biology. 2005; 151:182–195. [PubMed: 16043363]
15. Kulesa PM, Fraser SE. Cell dynamics during somite boundary formation revealed by time-lapse analysis. Science. 2002; 298:991–995. [PubMed: 12411697]
16. Rifes P, et al. Redefining the role of ectoderm in somitogenesis: a player in the formation of the fibronectin matrix of presomitic mesoderm. Development. 2007; 134:3155–3165. [PubMed: 17670788]
17. Zamir EA, Rongish BJ, Little CD. The ECM moves during primitive streak formation--computation of ECM versus cellular motion. PLoS Biol. 2008; 6:e247. [PubMed: 18922043]
18. Zamir EA, Czirok A, Cui C, Little CD, Rongish BJ. Mesodermal cell displacements during avian gastrulation are due to both individual cell-autonomous and convective tissue movements. Proc Natl Acad Sci U S A. 2006; 103:19806–19811. [PubMed: 17179040]
19. Berg, HC. Random Walks in Biology. Princeton Unversity Press; Princeton: 1993.
20. Czirok A, Zamir EA, Filla MB, Little CD, Rongish BJ. Extracellular matrix macroassembly dynamics in early vertebrate embryos. Curr Top Dev Biol. 2006; 73:237–258. [PubMed: 16782461]
21. Amaya E, Musci TJ, Kirschner MW. Expression of a dominant negative mutant of the FGF receptor disrupts mesoderm formation in Xenopus embryos. Cell. 1991; 66:257–270. [PubMed: 1649700]
22. Ciruna B, Rossant J. FGF signaling regulates mesoderm cell fate specification and morphogenetic movement at the primitive streak. Dev Cell. 2001; 1:37–49. [PubMed: 11703922]
23. Sun X, Meyers EN, Lewandoski M, Martin GR. Targeted disruption of Fgf8 causes failure of cell migration in the gastrulating mouse embryo. Genes Dev. 1999; 13:1834–1846. [PubMed: 10421635]
24. Watanabe T, et al. Tet-on inducible system combined with in ovo electroporation dissects multiple roles of genes in somitogenesis of chicken embryos. Dev Biol. 2007; 305:625–636. [PubMed: 17359965]
25. Cai AQ, Landman KA, Hughes BD. Modelling directional guidance and motility regulation in cell migration. Bulletin of mathematical biology. 2006; 68:25–52. [PubMed: 16794920]
26. Gillespie DT. Exact Stochastic Simulation of Coupled Chemical-Reactions. Journal of Physical Chemistry. 1977; 81:2340–2361.

27. Chapman SC, Collignon J, Schoenwolf GC, Lumsden A. Improved method for chick whole-embryo culture using a filter paper carrier. Dev Dyn. 2001; 220:284–289. [PubMed: 11241836]

28. Czirok A, Rupp PA, Rongish BJ, Little CD. Multi-field 3D scanning light microscopy of early embryogenesis. Journal of microscopy. 2002; 206:209–217. [PubMed: 12067365]

29. Rupp PA, Rongish BJ, Czirok A, Little CD. Culturing of avian embryos for time-lapse imaging. Biotechniques. 2003; 34:274–278. [PubMed: 12613250]

30. Araki I, Nakamura H. Engrailed defines the position of dorsal di-mesencephalic boundary by repressing diencephalic fate. Development. 1999; 126:5127–5135. [PubMed: 10529429]

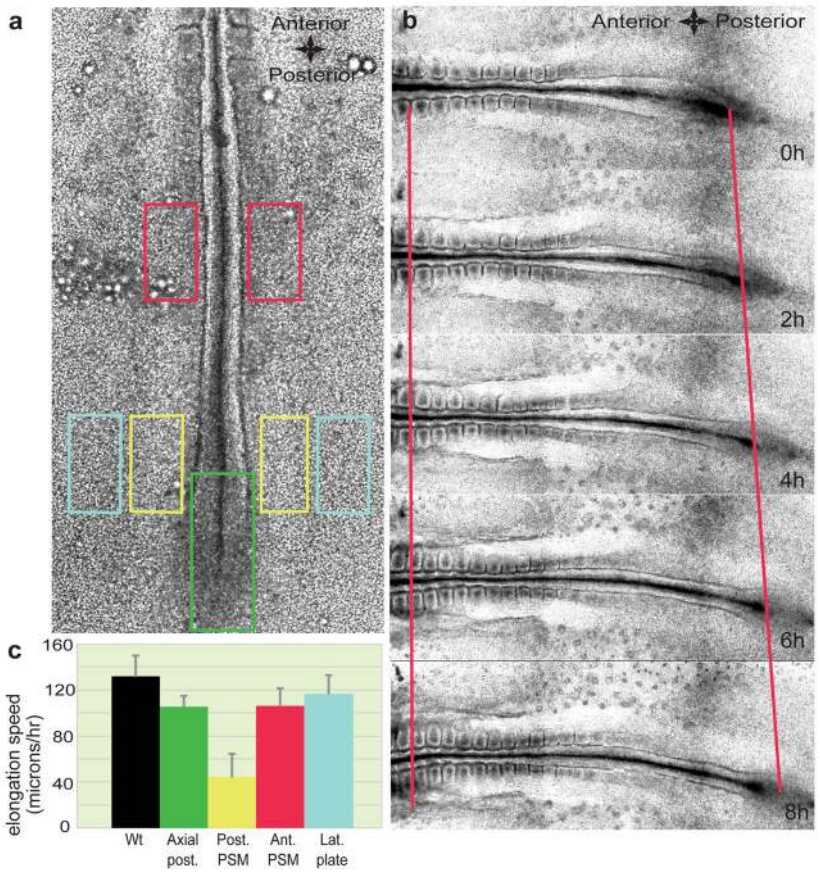

Figure 1. Role of caudal PSM in embryo elongation

a, Position of the ablations of the posterior PSM (yellow rectangles), lateral plate mesoderm (light blue rectangles), caudal axial tissue (green rectangle) and anterior PSM (red rectangles) in a stage HH11 embryo. **b**, Snapshot of different time points (during an 8-hour time period) showing elongation (red lines) of a wild type (Wt) embryo starting at stage HH11. The left red line denotes the level of somite 3, while the right red line denotes the level of Hensen's node. **c**, Elongation speed measurements. Error bars indicate the standard deviations. The black histogram corresponds to the elongation rate of non-ablated Wt embryos.

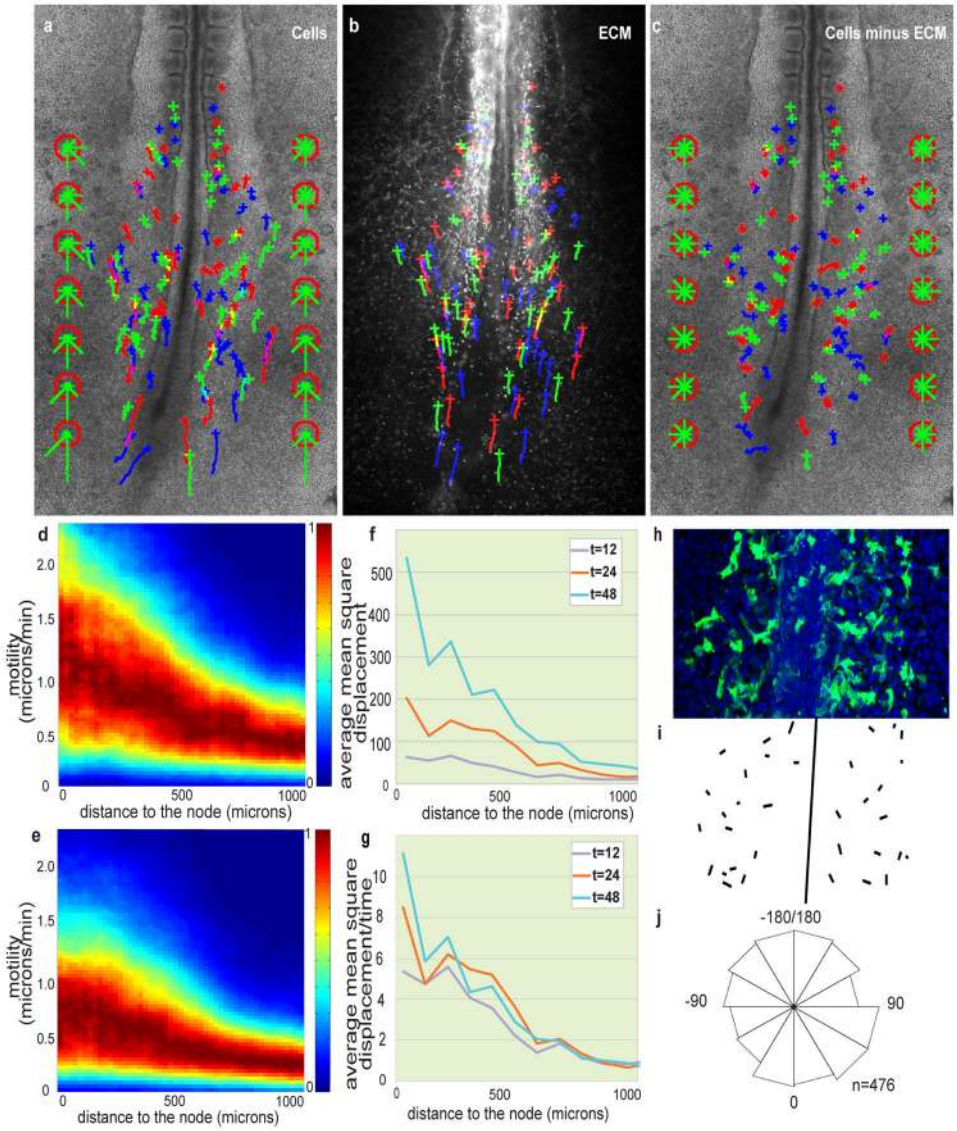

Figure 2. Posterior-to-anterior decreasing gradient of random motility in the PSM

a–c, H2B-GFP electroporated embryos injected with labelled anti-Fibronectin antibodies. Crosses represent cell position at $t = 0$; trajectories are represented by green, blue and red lines. The green bars in the red octagons represent cell directionality (see Supplementary Methods). **a,** Tracking of cellular movements. **b,** Tracking of ECM movement (Fibronectin). **c,** Cell movements after subtraction of ECM motion. **d, e,** Cellular motility along the AP axis with respect to a somite; node position is on the left; normalized probabilities for different motilities are colour coded (see Supplementary Methods). **d,** Gradient of cellular motility. **e,** Gradient of cellular motility relative to the ECM. **f,** Analysis of the mean square displacement of cells relative to the ECM along the AP axis as a function of time (in min.). **g**, Mean square displacement normalized by time (in min.). **h–j,** Orientation of cellular protrusions relative to the AP axis. **h,** Ventral view of the caudal part of an embryo electroporated with membrane-GFP. **i,** Representation of the orientations of major lamelliform protrusion. **j,** Rose diagram representing the distribution of the angles between

the major cellular lamelliform protrusion and the AP body axis (n = 476 cells from 14 different embryos, 0 degrees corresponds to a protrusion parallel to the AP axis and pointing toward the tail).

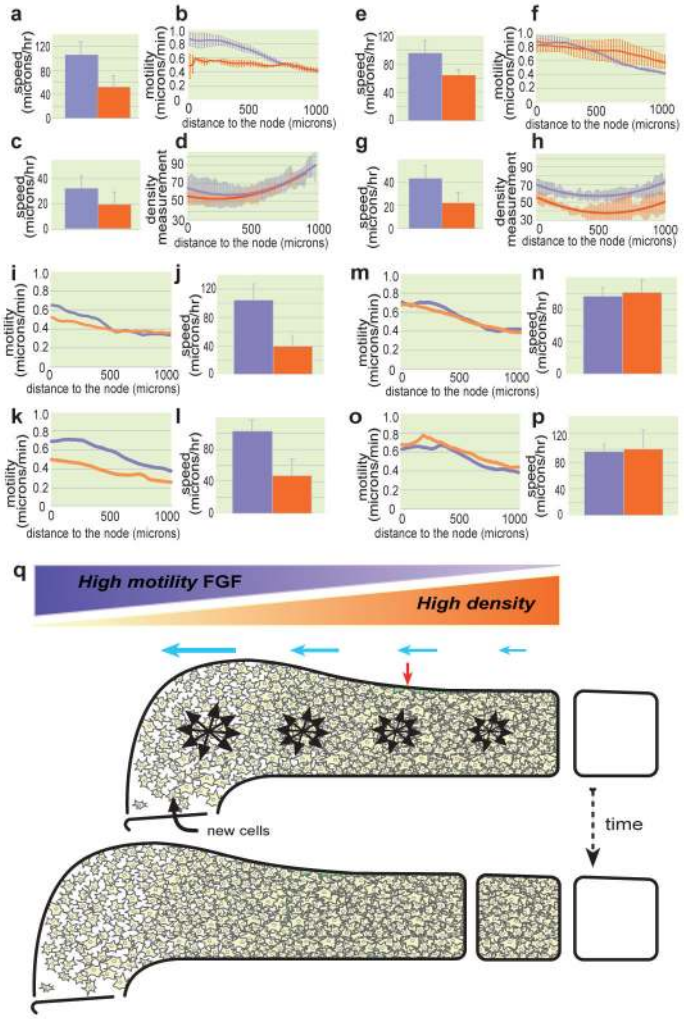

Figure 3. Effect of FGF signaling, cell movement and cell proliferation on axis elongation

a–p, Control (lavender) and treated (orange) conditions. **a, e, j, l, n, p,** Quantification of elongation. **c, g,** Convergence analysis. **b, f, i, k, m, o,** Mean cellular motility analysed along the AP axis. **d, h,** Analysis of PSM cellular density along the AP axis. The solid line represents a curve fitted to the mean value and the standard deviation is represented by the corresponding light-colored bars (*n*=4 or 5 for each condition). **a–d,** Inducible FGFR1dn electroporation. **e–h,** FGF8 electroporation. **i,j,** Y27632 treatment. **k,l,** Blebbistatin treatment. **m,n,** Aphidicolin treatment. **o,p,** Mitomycin treatment. **b,f** mean of two [for FGFR1dn] or three embryos [for FGF8]; errors bars represent the standard deviation). **q,** Model of the control of elongation by a gradient of random cellular motion in the PSM. Dorsal view of a schematic representation of the left PSM at two consecutive stages of embryo elongation. While new cells are entering the PSM, the gradient of random motility (lavender gradient; black arrow clusters) opposed to the gradient of cellular density (orange gradient) creates a directional bias in elongation (blue arrows) toward the posterior part of the tissue. This posterior expansion induces the convergence of the PSM tissue (red arrow).